Intrinsic Distribution of Magnetic Anisotropy in Thin Films Probed by Patterned Nanostructures

T. Thomson,* G. Hu, and B. D. Terris

Hitachi Global Storage Technologies, San Jose Research Center, 650 Harry Road, San Jose, California 95120, USA

(Received 26 September 2005; published 29 June 2006)

We demonstrate that the switching field distribution (SFD) in arrays of 50 nm to 5 μm Co/Pd elements, with perpendicular anisotropy, can be explained by a distribution of intrinsic anisotropy rather than any fabrication related effects. Further, simulations of coercivity and SFD versus element size allow the distribution of intrinsic anisotropy to be quantified in highly exchanged coupled thin films where the reversal mechanism is one of nucleation followed by rapid domain wall motion.

DOI: 10.1103/PhysRevLett.96.257204 PACS numbers: 75.30.Gw, 75.40.Mg, 75.50.Ss, 75.60.Jk

Nanomagnetic materials are now an extremely active area of research interest as evidenced by recent advances in high anisotropy nanoparticles [1], single-domain magnetic dots for logical operations [2], and spin manipulation devices [3]. This intense activity is driven partly by the huge potential of nanomagnetism-based materials in new applications from high density magnetic data storage, through magnetic logic and computation to biomagnetic functionality. An important aspect of nanoscale magnetism is the switching field distribution (SFD) of arrays of nanomagnetic elements. An element-to-element variation in anisotropy affects both the required reversal field, such as in continuous [4] or patterned [5] magnetic recording media and magnetic random access memory devices [6], as well as reversal dynamics, such as observed in spin torque excitations [7].

The SFD is influenced by distributions of fundamental physical and intrinsic magnetic properties including anisotropy, magnetization, exchange, and magnetostatic coupling [8,9], as well as by extrinsic properties such as variations in element sizes and element edge effects [10]. In continuous films consisting of isolated grains the width of the hysteresis loop is a direct reflection of the SFD, minus corrections from the neighboring grain demagnetizing fields. However, for patterned single-domain islands, it is usually highly exchange coupled systems which are of interest as these are most likely to lead to single-domain islands. The magnetic switching in these systems is generally assumed to one of nucleation of a small reversed volume followed by rapid domain wall propagation [11,12]. The hysteresis loops of such systems do not contain information about the underlying distribution of anisotropy associated with each nucleation volume, since once the weakest anisotropy nucleation volumes have reversed the remaining film can switch by domain wall propagation. Thus all nucleation fields (H_n) greater than the depinning field (H_p) do not participate in the reversal process.

While it might be assumed that sharp hysteresis loops and high levels of exchange coupling would lead to arrays of patterned islands with narrow SFD's, this is not what has been found experimentally where a SFD much broader than the limit imposed by magnetostatic fields is observed [11,13]. One might expect that any effects introduced by the fabrication process, such as element-to-element size variations or edge effects, would be minimized in highly exchange coupled systems. We demonstrate below that the SFD of the patterned islands is a reflection of the spatial variation of the continuous film's nucleation volume SFD, assuming that the material on island arrays is identical to the continuous films. Thus, controlling the SFD of nucleation volumes is key to obtaining arrays of patterned islands with narrow SFD's. Alternatively, patterned island arrays may offer the opportunity to measure the continuous film nucleation volume SFD. To our knowledge, this distribution is not otherwise accessible as it is usually masked by the domain wall depinning field.

One particular material system that has received significant scientific and technological attention is that of Co/Pt or Co/Pd based multilayers. These materials have perpendicular magnetic anisotropy and are highly exchange coupled. We have fabricated arrays of magnetic islands (pillars) by depositing Co/Pd multilayer films onto prepatterned Si/SiO_2 substrates. Co/Pd multilayer films with a structure of Si/SiO_2/Pd(3 nm)/$[$Co(0.33 nm)/Pd(0.96 nm)$]_8$/Pd(2 nm) were dc sputtered at room temperature using an Ar pressure of 3 mTorr [13]. Depositing onto prepatterned substrates gives arrays of magnetically isolated islands separated by a network of trenches. The substrates were patterned using electron beam lithography to create islands on length scales from a few tens of nanometers, a length scale characteristic in magnetism [9], e.g., exchange length ($l_{\mathrm{ex}} = \sqrt{\frac{A}{2\pi M_s^2}} = 17$ nm–24 nm for the Co/Pd multilayers reported here, assuming an exchange constant $A = 3$–6×10^{-6} erg/cm and saturation magnetization $M_s = 400$ emu/cm^3), to hundreds of microns which should be representative of the continuous film. The magnetic properties of the island arrays and continuous films were determined using the polar magneto-optic Kerr effect (MOKE) at a wavelength of 633 nm, magnetic force microscopy (MFM), and of the continuous films by vibrating sample magnetometry.

Small islands fabricated in this manner exhibit a Stoner-Wohlfarth (S-W) reversal behavior. While the continuous

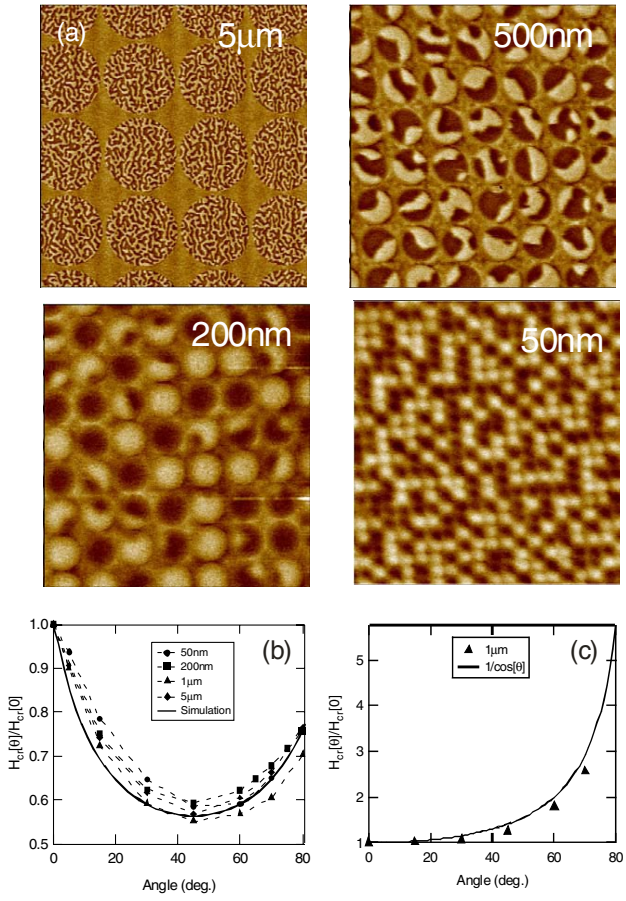

FIG. 1 (color online). MFM images showing the magnetic state of 50 nm to 5 μm islands following ac demagnetization. A multidomain ground state is clearly visible for islands 200 nm and greater; (b) H_{cr} as a function of applied field angle normalized to H_{cr} at $\theta = 0$ for different island sizes. The thick solid line is a simulation of the angle dependence of H_{cr} assuming a Gaussian distribution of anisotropy axes with a sigma of 2 degrees; (c) H_{cr} as a function of applied field angle normalized to H_{cr} at $\theta = 0$ for 1 μm size islands with prereversed nucleation sites.

film remanent coercivity (H_{cr}), defined as the reverse field required to reduce the remanent magnetization to zero, is typically a few hundred Oe, the small, 50–100 nm diameter, islands have a MOKE measured H_{cr} of 5500–6500 Oe. Since the network of trenches reverse in a field similar to continuous films, the signal from the islands can be separated easily [13]. These results are consistent with a model whereby the continuous film reverses by nucleation of a low anisotropy volume followed by rapid domain wall propagation. The small islands reverse by rotation and the coercivity is determined by the island anisotropy [14]. Figure 1(a) shows MFM images of ac demagnetized island arrays for four island sizes. ac demagnetizing allows the island arrays to obtain an approximate ground state and the images for 5 μm, 500 nm, and 200 nm island sizes show a multidomain structure. The 50 nm island size does not support a stable multidomain configuration. Further evidence for reversal by rotation in small elements can be seen by investigating the angle dependence of H_{cr}, as shown in Fig. 1(b), by applying the magnetic field at an angle θ with respect to the normal. While the continuous film (not shown) has the well-known $1/\cos(\theta)$ dependence, indicative of wall propagation limited reversal, the small islands display a S-W-like dependence with a minimum H_{cr} at 45 degrees.

However, as also shown in Fig. 1(b), even islands up to 5 μm in size, which cannot reverse by rotation, can show a S-W-like angle dependence. These islands can support domain walls and one might expect their properties to begin to resemble continuous films and thus reverse by a nucleation and wall propagation process. However, if $H_n > H_p$ the measured angle dependence is that of the small S-W nucleation volume, as observed. Further evidence for this model is seen in experiments where reversed regions are introduced into islands capable of supporting a domain wall by applying a large in-plane magnetic field [15]. Islands containing reversed regions have $H_n = 0$ and H_{cr}, now determined by H_p, closer to that of the continuous film, as would be expected for island reversal that depends on the depinning field. The complete switching of such islands with reversed regions is then governed by wall depinning, and indeed the angle dependence is $1/\cos(\theta)$, as shown in Fig. 1(c).

Figure 2 shows experimental data together with simulated results for H_{cr} and the width (standard deviation) of the SFD, determined by differentiating remanence curves, as a function of island size. The SFD of these arrays can be simulated as follows: we assume, as hypothesized above, that each island switches by the reversal of a small nucleation volume followed by rapid domain wall motion. The applied field required for nucleation depends on the local anisotropy at the nucleation volume and the total effective field acting on the nucleation volume. The uniaxial anisotropy constant (K_u) can be separated into an intrinsic term

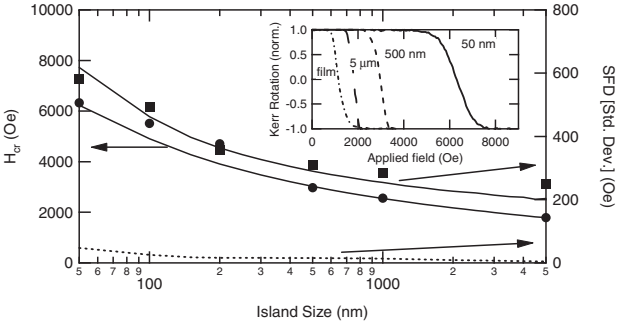

FIG. 2. Left-hand axis: coercivity of island arrays as a function of island size (●) and results of simulation (solid line). Right hand axis: switching field distribution characterized by its standard deviation (■) and results of simulation (solid line). Also shown is the SFD standard deviation (dashed line) due only to differences in magnetostatic environment, i.e., due to switching of neighboring islands. The inset shows remanence curves for three island sizes and the continuous film.

($K_{\rm int}$) and shape term (K_s), where the intrinsic part includes contributions from magnetocrystalline, interfacial, and stress anisotropies

$$K_u(x, y) = K_{\rm int}(x, y) + K_s. \quad (1)$$

Since our goal is to compare simulated results with measured data, the effects of finite measurement times and temperatures are accounted for using the Sharrock formalism [16],

$$H_{\rm cr}(t, T) = \frac{2[K_{\rm int}(x, y) + K_s]}{M_s} \times \left\{1 - \left[\frac{[K_{\rm int}(x, y) + K_s]V}{k_B T} \ln\left(\frac{f_0 t}{\ln(2)}\right)\right]^{1/2}\right\}, \quad (2)$$

where k_B is the Boltzmann constant , T the absolute temperature, f_0 is the characteristic frequency taken as 10^{10} Hz, t is the time, and V is the nucleation volume.

The variation of the intrinsic anisotropy $K_{\rm int}(x, y)$ is assumed to have a Gaussian form such that the probability of a particular value of $K_{\rm int}$ for a given nucleation volume is determined by $P[K_{\rm int}(x, y)]$, where

$$P[K_{\rm int}(x, y)] = \frac{1}{\sigma_{K\rm int}\sqrt{2\pi}} \exp\left(-\frac{[K_{\rm int}(x, y) - K_{\rm int}^{\rm mean}]^2}{2\sigma_{K\rm int}^2}\right). \quad (3)$$

It is assumed that the nucleation volumes are randomly distributed in the x-y plane in discrete units set by the nucleation length ($l_{\rm nuc}$) defined by $V = {l_{\rm nuc}}^2 z$, where z is the film thickness. $\sigma_{K\rm int}$ is the width of the distribution of intrinsic anisotropy.

This model requires M_s and $K_{\rm int}^{\rm mean}$ as input parameters which, under the assumption that material deposited on island arrays and flat surfaces is magnetically the same, are experimentally accessible quantities. The value of M_s is determined assuming a uniform magnetization throughout the entire multilayer thickness. The shape anisotropy term K_s determined by the island geometry and calculated using the method of Aharoni [17] with the assumption that each island is homogeneously magnetized. $K_{\rm int}^{\rm mean}$ for the continuous film is determined by measuring the in-plane magnetic field, H_k, required to saturate the magnetization (hard axis method) where $H_k = 2(K_{\rm int}^{\rm mean} + K_s)/M_s$ with $K_s = 4\pi M_s$. A more rigorous micromagnetic calculation of K_s would further improve the model but is unlikely to change the results significantly. This leaves the nucleation volume V and $\sigma_{K\rm int}$ as the only two parameters not directly measurable. An estimate of 30 nm for the nucleation length, obtained from micromagnetic modeling [18], is used as a starting point for our simulations.

The agreement between the data and simulation (Fig. 2) is immediately apparent with a single set of parameters describing the reversal behavior of a wide range of island sizes. Contributions from neighboring islands which lead to a widening of the switching field distribution and set a limit on the minimum switching field distribution are not included in the simulation. In these island arrays the contribution from neighboring islands to the width of the SFD is minor and is comparable to the experimental uncertainties in determining the width of the SFD. The values used for the simulation are $M_s = 400\,{\rm emu/cm^3}$, $K_{\rm int}^{\rm mean} = 2.20 \times 10^6\ {\rm erg/cm^3}$, $\sigma_{K\rm int}/K_{\rm int}^{\rm mean} = 0.076$ with $l_{\rm nuc} = 38$ nm.

Figure 3 shows measured SFD's determined by differentiating the island array dc demagnetizing remanence curves and simulated SFD's for the 50 nm and 1 μm island arrays. The simulation not only reproduces $H_{\rm cr}$ and standard deviation parameters correctly, it also gives the functional form of the reversal and the systematic changes in functional form as island size increases, from a near Gaussian distribution for small (50 nm), islands, to a more log-normal form observed for large (1 μm) islands.

$H_{\rm cr}$ as a function of field exposure time is shown in Fig. 4 for arrays of three island sizes, 50 nm, 500 nm, and 5 μm, along with simulation results obtained using the parameters found previously. The simulations allow H_0 to be estimated, where H_0 is defined as the switching field in the absence of thermal activation effects and is the switching field needed at time scales on the order of $1/f_0$. As a check on the validity of these H_0 values we plot, on the extreme left-hand side of the figure, values of the applied in-plane field necessary to introduce a reversed region in every island of the array. Effectively this is the site in each island with the lowest local $K_{\rm int}$. Of course, the micromagnetic details of the creation of small reverse regions are complex but given the large range of reversal fields here, it does provide a consistency check which agrees well with

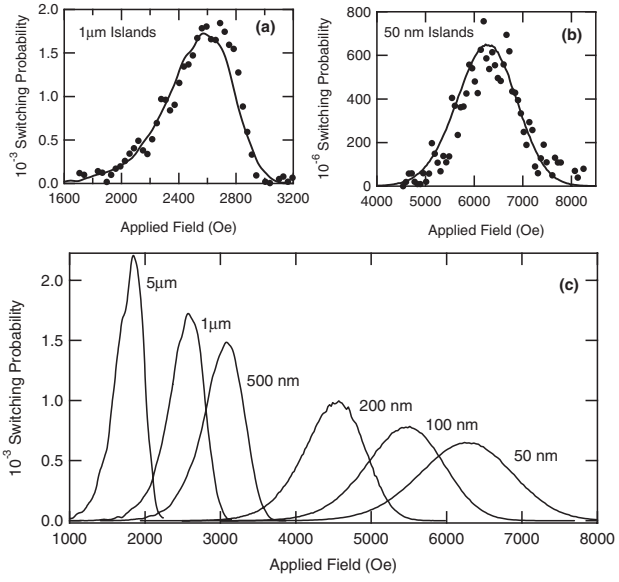

FIG. 3. SFD data (markers) from differentiated dc demagnetizing remanence curves and simulations (lines) for (a) 1 μm island arrays, (b) 50 nm island arrays, and (c) a summary of the simulated SFD's as a function of island size. Note how the change in functional form, as island size increases, is reproduced in the simulations.

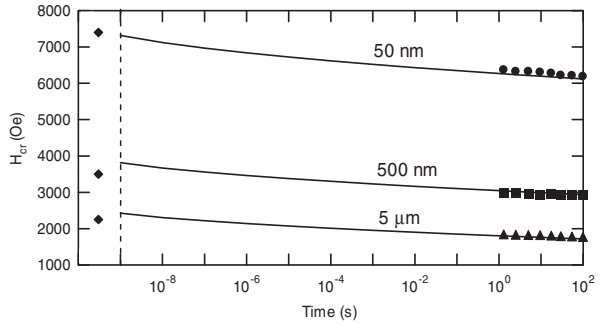

FIG. 4. Right of dotted line: data (markers) and simulation (lines) results for the time dependence of remanent coercivity for 50 nm, 500 nm, and 5 μm island arrays. Left of dotted line: 50 nm islands, H_0 estimated from H_k; 500 nm and 5 μm islands, values of H_0 estimated from in-plane field necessary to introduce reversed sites into the island arrays.

the H_0 values obtained from the simulations. The fact that the curves for different island sizes extrapolate to different values of H_0 is also justification for our assumption that the SFD is due to $\sigma_{K\text{int}}$ as opposed to a distribution of nucleation volumes. If the SFD was due to a distribution of nucleation volumes, then all islands should have the same H_0, since the effect of a distribution of nucleation volumes would only be observable at finite temperatures, and times greater than $1/f_0$.

We have demonstrated that island reversal data can be accurately simulated using a distribution of intrinsic anisotropy, and that the island SFD is not a result of patterning, as often supposed. These results raise the question as to the source of the anisotropy distribution. A distribution of easy axes angles can be discounted as a major contributor. If the SFD was due to a distribution of easy axis angles, then applying fields at different angles would lead to an apparent change in SFD width due to the highly nonlinear form of the S-W curve, particularly around 0 degrees, and we do not observe such a change. Local fluctuations in Co concentration offer a potential explanation as the interfacial anisotropy is very sensitive to Co layer thickness. However, it is unclear how such an explanation would work in detail as for the nucleation length found here, there are many thousands of Co atoms per layer (38 nm $\times$ 38 nm $\approx$ 30 000 atoms) and one might anticipate that this contains all possible local atomic configurations. Variations associated with the grain structure certainly could be responsible as grain sizes are typically in the range 5–20 nm. The local variation in anisotropy could also be a result of variations in stress, for example, Hong *et al.* [19] recently proposed that stressed interfacial alloying played an important role in creating perpendicular anisotropy in Co/Pd multilayer films. While the exact nature of the underlying source of the intrinsic anisotropy distribution remains to be fully explained, the ability to accurately characterize it using the methods demonstrated has wide application in nanomagnetic systems.

The authors wish to thank C. T. Rettner of the IBM Almaden Research Center for help with sample fabrication.

*Email address: thomas.thomson@hitachigst.com

[1] S. Sun, C. B. Murray, D. Weller, L. Folks, and A. Moser, Science **287**, 1989 (2000).
[2] D. A. Allwood, G. Xiong, C. C. Faulkner, D. Atkinson, D. Petit, and R. P. Cowburn, Science **309**, 1688 (2005).
[3] J. A. Katine, F. J. Albert, R. A. Buhrman, E. B. Myers, and D. C. Ralph, Phys. Rev. Lett. **84**, 3149 (2000).
[4] J-G. Zhu, Y. Peng, and D. E. Laughlin, IEEE Trans. Magn. **41**, 543 (2005).
[5] B. D. Terris and T. Thomson, J. Phys. D **38**, R199 (2005).
[6] B. N. Engel *et al.*, IEEE Trans. Magn. **41**, 132 (2005).
[7] W. H. Rippard, M. R. Pufall, S. Kaka, S. E. Russek, and T. J. Silva, Phys. Rev. Lett. **92**, 027201 (2004); A. A. Tulapurkar, Y. Suzuki, A. Fukushima, H. Kubota, H. Maehara, K. Tsunekawa, D. D. Djayaprawira, N. Watanabe, and S. Yuasa, Nature (London) **438**, 339 (2005); F. B. Mancoff, N. D. Rizzo, B. N. Engel, and S. Tehrani, Nature (London) **437**, 393 (2005).
[8] J. Ferré, in *Spin Dynamics in Confined Magnetic Structures I*, edited by B. Hillebrands and K. Ounadjela (Springer-Verlag, Berlin, 2002).
[9] A. Hubert and R. Schäfer, *Magnetic Domains: The Analysis of Magnetic Microstructures* (Springer-Verlag, Berlin, 1998).
[10] M. T. Bryan, D. Atkinson, and R. P. Cowburn, Appl. Phys. Lett. **85**, 3510 (2004).
[11] Y. Kitade, H. Komoriya, and T. Maruyama, IEEE Trans. Magn. **40**, 2516 (2004); C. T. Rettner, S. Anders, T. Thomson, M. Albrecht, Y. Ikeda, M. E. Best, and B. D. Terris, IEEE Trans. Magn. **38**, 1725 (2002); S. P. Li, A. Lebib, Y. Chen, Y. Fu, and M. E. Welland, J. Appl. Phys. **91**, 9964 (2002); H-J. Jang, P. Eames, E. D. Dahlberg, M. Farhoud, and C. A. Ross, Appl. Phys. Lett. **86**, 023102 (2005); S. Landis, B. Rodmacq, and B. Dieny, Phys. Rev. B **62**, 12 271 (2000); V. Mathet, T. Devolder, C. Chappert, J. Ferré, S. Lemerle, L. Belliard, and G. Guentherodt, J. Magn. Magn. Mater. **260**, 295 (2003).
[12] J-P. Jamet, S. Lemerle, P. Meyer, J. Ferré, B. Bartenlian, N. Bardou, C. Chappert, P. Veillet, F. Rousseaux, D. Decanini, and H. Launois, Phys. Rev. B **57**, 14 320 (1998).
[13] G. Hu, T. Thomson, M. Albrecht, M. E. Best, B. D. Terris, C. T. Rettner, S. Raoux, G. M. McClelland, and M. W. Hart, J. Appl. Phys. **95**, 7013 (2004).
[14] G. Hu, T. Thomson, C. T. Rettner, S. Raoux, and B. D. Terris, J. Appl. Phys. **97**, 10J702 (2005).
[15] G. Hu, T. Thomson, C. T. Rettner, and B. D. Terris, IEEE Trans. Magn. **41**, 3589 (2005).
[16] M. P. Sharrock and J. T. McKinney, IEEE Trans. Magn. **17**, 3020 (1981).
[17] A. Aharoni, J. Appl. Phys. **83**, 3432 (1998).
[18] R. Dittrich, G. Hu, T. Schrefl, T. Thomson, D. Suess, B. D. Terris, and J. Fidler, J. Appl. Phys. **97**, 10J705 (2005).
[19] J. I. Hong, S. Sankar, A. E. Berkowitz, and W. F. Egelhoff, Jr., J. Magn. Magn. Mater. **285**, 359 (2005).